Creating a low-symmetry insulating, ferroelectric, and antiferromagnetic material from a high-symmetrical metallic ferromagnet via defect engineering: The case of LaBaCo$_2$O$_{5+\delta}$ compounds

Yurong Yang,[1] Chunrui Ma,[2,3] Ming Liu,[4] Hong Jian Zhao,[1,5] Yuan Lin,[6] Chonglin Chen,[3] and L. Bellaiche[1]

[1]*Physics Department and Institute for Nanoscience and Engineering, University of Arkansas, Arkansas 72701, USA*
[2]*State Key Laboratory for Mechanical Behavior of Materials, Xi'an Jiaotong University, Shaanxi 710049, People's Republic of China*
[3]*Department of Physics and Astronomy, University of Texas at San Antonio, Texas 78249, USA*
[4]*Electronic Materials Research Laboratory, Key Laboratory of the Ministry of Education and International Center for Dielectric Research, Xi'an Jiaotong University, Shaanxi, 710049, People's Republic of China*
[5]*Laboratory of Dielectric Materials, School of Materials Science and Engineering, Zhejiang University, Zhejiang, 310027, People's Republic of China*
[6]*State Key Laboratory of Electronic Thin films and Integrated Devices, University of Electronic Science & Technology of China, Sichuan 610054, People's Republic of China*

First-principles calculations are performed to investigate the properties of defect-free LaBaCo$_2$O$_6$ materials as well as LaBaCo$_2$O$_5$ films possessing ordered oxygen vacancy structures. These calculations predict that the defect-free LaBaCo$_2$O$_6$ crystallizes in a tetragonal state with an axial ratio smaller than unity, and is metallic and ferromagnetic as consistent with the literature. In contrast, the LaBaCo$_2$O$_5$ film adopts a low-symmetry monoclinic state having an axial ratio larger than 1, is insulating and even ferroelectric, as well as exhibits a G-type antiferromagnetic ordering. Our calculations further reveal the origin of these defect-induced changes in properties. Moreover, further experiments we conducted demonstrate the possibility to grow highly epitaxial LaBaCo$_2$O$_5$ films with ordered oxygen vacancies, via reduction treatments, and confirm some of our predictions. These findings can open a new avenue for the design and synthesis of multiferroics via defect engineering.

I. INTRODUCTION

Cobalt oxides have been widely studied for many years due to their high chemical stability, excellent oxygen permeability, and many other unique physical chemistry properties for energy conversion, catalysts, sensors, and solid oxide fuel cells, etc. [1–4]. They also exhibit rich magnetic and electronic transport properties, ranging from paramagnetism to ferromagnetism via antiferromagnetism, from magnetic frustration to metal-insulator transition and colossal magnetoresistance, and many others [5–7]. These phenomena are highly dependent upon the degrees of freedom such as charge distribution, spin and orbital orderings, and lattice structures [8]. In addition, cobalt oxides can possess different cobalt and oxygen coordination from tetrahedral, pyramidal to octahedral depending on its oxygen content, which leads to various crystal structures having a great flexibility of the oxygen frameworks [9]. As a result, oxygen nonstoichiometry is a crucial parameter for tuning physical properties determined by their crystal structure [10]. Among the cobalt oxide family, LaBaCo$_2$O$_{5+\delta}$ (with $0 \leqslant \delta \leqslant 1$) (LBCO) exhibit anomalous physical properties such as giant magnetoresistance effect, superfast chemical dynamics, etc. [11–14]. Moreover, the achievement of fabricating (with various postannealing treatments) an *ordered oxygen vacancy structure* in another related material, namely, highly epitaxial (La,Sr)CoO$_{3-\delta}$ thin films, has opened up a new avenue for the studies of the ordered oxygen vacancy structures in Co-based systems [3,15]. In particular, one may wonder if the formation of such structures with vacancies can dramatically alter the properties of LBCO compounds, which are known to be metallic and ferromagnetic, within a tetragonal state having an axial ratio smaller than 1, when no or few oxygen vacancies exist in the materials [16,17].

The goal of this paper is to address this issue, by first performing and analyzing first-principles calculations. It is found that the creation of ordered oxygen vacancies inside LBCO does result in original properties. Examples include the system becoming insulating, ferroelectric and antiferromagnetically-ordered, in addition to adopting a low-symmetry monoclinic phase having an axial ratio larger than 1. The reasons behind such defect-induced changes are also unraveled. Finally, experiments are further conducted to demonstrate that the formation of ordered oxygen vacancies can occur inside high-epitaxial LBCO films and to confirm some of our striking predictions, which is promising for opening a route aimed at designing novel properties and multiferroics via defect-engineering.

II. METHODS

In the present study, we perform first-principles calculations on two different types of LBCO supercells. The first type concerns the "defect-free" LaBaCo$_2$O$_6$ system, and is schematized in Fig. 1. Regarding the atomic arrangement of its *A* site atoms (La and Ba), it has pure La layers alternating, along the out-of-plane direction, with layers solely made of Ba. The second type of supercell is a LaBaCo$_2$O$_5$ structure and possesses (ordered) oxygen vacancies. Its supercell contains 10 O, 4 Co, 2 Ba, and 2 La atoms, different *A* site atoms orderings are considered (see Fig. 2). The in-plane and out-of-plane lattice vectors and atomic positions are allowed to relax in order to minimize
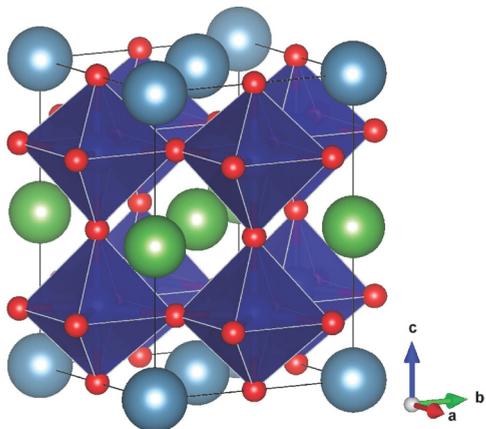
FIG. 1. Atomic structure used to mimic LaBaCo$_2$O$_6$ with no defect. The red, blue, green, and light blue spheres represent O, Co, La, and Ba ions, respectively.

the total energy and obtain forces smaller than 0.001 eV/Å on any ions. Practically, atomic relaxation and calculations of properties are carried out using density functional theory (DFT) within the framework of PBEsol $+ U$ [18,19] and the projector augmented-wave potentials, as implemented in the VASP code [20]. The Hubbard U value for Co atoms is chosen to be $U = 2.5$ eV. Note that we also tested values of U equal to 2, 3, 4, 5, 6, 7, and 8 eV within PBEsol $+ U$, as well as the Heyd-Scuseria-Ernzerhof hybrid functionals [21]. All these different U values give the same antiferromagnetic ground state, lead to an insulating character, and very similar

magnetic moment on Co atoms with those discussed and reported here (for PBEsol $+ U$ with $U = 2.5$ eV) in the case of LaBaCo$_2$O$_6$. The energy cutoff is selected to be 550 eV, and the k-point mesh is taken to be $6 \times 6 \times 4$. The polarization is calculated by the Berry phase method [22]. Moreover, spin-orbit coupling and noncollinear magnetism are considered in order to investigate some magnetic properties of the defectuous LBCO.

III. RESULTS

A. Properties of LaBaCo$_2$O$_6$

The defect-free LBCO (i.e., LaBaCo$_2$O$_6$) compound is predicted here to adopt a tetragonal symmetry with a *P4/mmm* space group (as a result of its layered structure), with an in-plane and out-of-plane lattice constants of 3.90 and 7.527 Å, respectively, which yield a normalized axial ratio of $c/a = 0.965$, which is smaller than 1. Our *ab initio* calculations also yield that this defect-free system is metallic and is a ferromagnet having a spontaneous total magnetization of 2.5 μ_B per five atoms, as consistent with Refs. [16,17] [note that (i) we numerically checked the energies of the ferromagnetic and C-, G-, and A-type antiferromagnetic orderings, and found the ferromagnetic (FM) structure to have the lowest energy in LaBaCo$_2$O$_6$; and (ii) the magnetization around each Co ions in the ferromagnetic state is found to be slightly smaller than 2.5 μ_B per five atoms, namely it is 2.2 μ_B, because oxygen and other ions also contribute to the total magnetization].
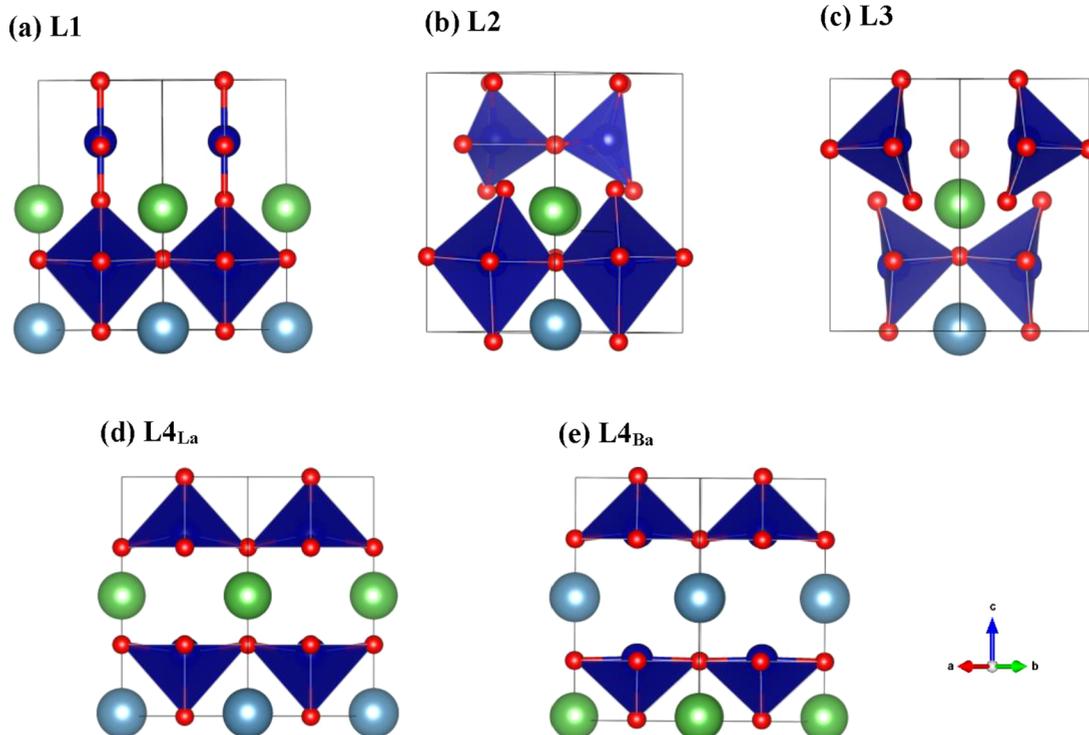
(a) L1 **(b) L2** **(c) L3**

(d) L4$_{La}$ **(e) L4$_{Ba}$**

FIG. 2. Chosen configurations for LaBaCo$_2$O$_5$ compounds having A-site ordering along [001] and deduced from a perovskite structure. These configurations contain 18 atoms per unit cell, and have lattice vectors $\boldsymbol{a}$ being along the [1$\bar{1}$0] pseudocubic direction, $\boldsymbol{b}$ being oriented along the pseudocubic [110] direction, and $\boldsymbol{c}$ being along the pseudocubic [001] direction. The red, blue, green and light blue spheres represent O, Co, La, and Ba ions, respectively.

TABLE I. Energies of different considered atomic structures of $LaBaCo_2O_5$ (deduced from the perovskite structure) with different magnetic configurations (in eV/f.u.). The zero of energy is chosen to correspond to the L2 structure adopting a G-type antiferromagnetism.

	G-AFM	C-AFM	A-AFM	FM
L1	0.462	0.434	0.414	0.255
L2	0.000	0.157	0.086	0.197
L3	0.422	0.102	0.409	0.362
L4$_{La}$	−0.110	−0.003	0.078	0.199
L4$_{Ba}$	1.094	1.335	0.937	1.433
RS1	0.785	0.894	0.571	0.536
RS2	0.043	0.163	0.111	0.218
RS3	0.755	0.898	0.809	0.838
RS4	0.900	0.966	1.089	1.178

B. Structure of $LaBaCo_2O_5$

Figure 2 depicts different presently considered structures all exhibiting ordering of La and Ba ions along the [001] direction. Configuration L1 is constructed from the bulk perovskite structure having the *I4cm* space group (which possesses $a^0a^0c^-$ oxygen octahedral tilting pattern and an electrical polarization along the [001] direction) by removing two O atoms in a (001) Co-O plane and then relaxing the resulting configuration. Configuration L2 is built the same way but by removing two nearest O atoms, and configuration L3 is built by removing one O atom in each (001) Co-O plane. Finally, Configurations L4$_{La}$ and L4$_{Ba}$ are constructed by removing O atoms in La-O and Ba-O planes, respectively (note that we also constructed similar configurations, but starting from cubic or R3c bulk perovskite, and obtained results that are similar to those starting from the I4cm space group of bulk perovskite). We also built structures we denote as RS1, RS2, RS3, and RS4 and that can be deduced from the L1, L2, L3, and L4 structures, respectively, by making the arrangements between La and Ba ions being of rocksalt type. Table I reports the total energy of all these relaxed configurations, further considering four different types of magnetic ordering

TABLE II. Energies of different Brownmillerite structures of $LaBaCo_2O_5$ with different magnetic configurations (in eV/f.u.). The zero of energy is chosen to correspond to the L2 structure adopting a G-type antiferromagnetism.

	G-AFM	C-AFM	A-AFM	FM
BM-L1	0.035	0.058	0.153	0.247
BM-L2	0.005	0.096	0.104	0.301
BM-L3	0.132	0.264	0.271	0.354
BM-RS	0.130	0.230	0.068	0.161

for each configuration: G-type antiferromagnetic (G-AFM), C-type antiferromagnetic (C-AFM), A-type antiferromagnetic (A-AFM), and ferromagnetic (FM).

We also built other configurations, still having a $LaBaCo_2O_5$ stoichiometry but adopting the Brownmillerite structure. These configurations are shown in Fig. 3 and their energies are indicated in Table II for the different aforementioned magnetic orderings. BM-L1 possesses one La-O layer and one Ba-O layer that alternate along the [001] direction. On the other hand, in BM-L2 and BM-L3, two neighboring layers La-O alternate with two neighboring Ba-O layers along [001], and BM-RS exhibits a rocksalt ordering between La and Ba atoms. Tables I and II reveal that the three lowest-in-energy structures are L2, L4$_{La}$, and BM-L2, and that they each prefer a G-type antiferromagnetism. Their axial ratio is numerically found to be 1.017, 0.953, and 0.983. In other words, L2 is the only lowest-in-energy structure that adopts an axial ratio that is larger than 1, which is precisely the type of axial ratio that our current measurements find (see Ref. [23], where an experimental value of 1.023 is reported for the axial ratio). Moreover, L2 has the same type of oxygen vacancies arrangement (namely, occurring in planes containing Co ions) with the one experimentally found and reported in Fig. 6. Therefore we choose L2 structure for investigating the properties in $LaBaCo_2O_5$. Note that L2 can be considered to be a novel structure since we are not aware that it has ever been reported before, unlike L4 [15,24] and the Brownmillerite structure [3,25]. Note also that we numerically
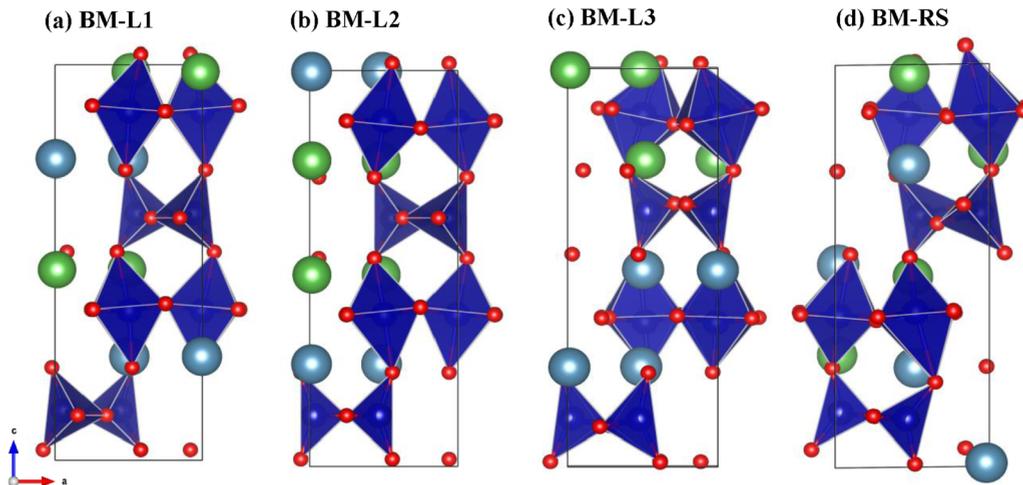

(a) BM-L1   **(b) BM-L2**   **(c) BM-L3**   **(d) BM-RS**

FIG. 3. Chosen Brownmillerite configurations for $LaBaCo_2O_5$ compounds having *A*-site ordering along [001] [(a)–(c)] and being of rocksalt type (d). The red, blue, green, and light blue spheres represent O, Co, La, and Ba ions, respectively.

found (not shown here) that L4$_{La}$ and BM-L2 have strongly unstable phonons when epitaxially grown on SrTiO$_3$ (as done in the experiments described below), which further explains why we focused on L2 in the manuscript. Furthermore, the fact that Table I indicates that L2 has a higher computed energy than L4$_{La}$ implies that L2 is a metastable state, rather than the ground state, at low temperature. Such state can either become the ground state at finite temperature or is accessible by measurements even if it is not the ground state, which would explain its experimental observation (see Ref. [23]).

C. Properties of LaBaCo$_2$O$_5$

The L2 structure of LaBaCo$_2$O$_5$ is found to have a monoclinic symmetry with a space group of Pc, and its computed in-plane lattice constants have a magnitude of 3.96 Å, while the out-of-plane lattice parameter is about 8.06 Å, which yields a normalized axial ratio of $c/a = 1.018$ (and which is thus larger than 1). It is also found to be insulating and to possess a polarization having an out-of-plane component (i.e., along the pseudocubic [00$\bar{1}$] axis) of about 1.3 μC/cm^2 of magnitude, and an in-plane component of about 6.1 μC/cm^2 along the pseudocubic [110] direction. Note that the fact that this polarization has both in-plane and out-of-plane components is consistent with the monoclinic symmetry of the ground state and that these components of the polarization can be altered by epitaxial strain. Moreover, the defectuous LBCO system presents a magnetic ordering that consists of a primary G-type antiferromagnetic vector lying along the [110] direction *and* a secondary ferromagnetic order being along the perpendicular [1$\bar{1}$0] direction, yielding a magnetization of about 0.04 μB per Co atoms. The latter, weak magnetization originates from the spin-orbit-induced canting of the magnetic moment of the tetrahedral Co ions. In other words, playing with oxygen vacancies in LBCO can transform the system from a ferromagnetic metal of tetragonal symmetry to a predominantly antiferromagnetic and insulating material possessing an electrical polarization altogether with a weak magnetization, and adopting a low-symmetry monoclinic ground state. Defect engineering in LBCO is therefore promising to alter and control various properties, and create new multiferroics.

Let us now concentrate on the out-of-plane component of the polarization of the L2 structure of LaBaCo$_2$O$_5$, that adopts a magnitude of about 1.3 μC/cm^2. To reveal its origin, Table III provides the polarization associated with the (001) La-O, Ba-O, Co-O$_2$ and Co-O layers and arising from the fact that the cation and oxygen atoms move away from each other in each of these four types of planes (i.e., these layers exhibit a rumpling). These polarizations are computed as the product between the effective charges of the ions and their displacement with

respect to their ideal positions. Table III reveals that the overall out-of-plane polarization of the defectuous LBCO system is pointing down and arises from the incomplete compensation between the dipole moments (i) formed around the Ba-O layers and those formed near the La-O layers; as well as those (ii) formed around the Co(T)-O layers (with Co being tetrahedral) and those formed near the Co(O)-O$_2$ layers (with Co being octahedral). Note that item (ii) is reminiscent of a result in Sr$_{1-x}$Ba$_x$MnO$_3$ [26] for which magnetic ions were found to contribute to the polarization. Moreover, items (i) and (ii) can also be understood by simple electrostatics. For that, let us first assume that the Co ions being in an octahedral environment are charged $+3$, while those being in a tetrahedral environment are charged $+2$ to ensure that LaBaCo$_2$O$_5$ is neutral (note that this assumption is not only consistent with the built-in polarization we computed by Berry phase in LaBaCo$_2$O$_5$, but also with the charges exhibited by octahedral and tetrahedral Co ions in Co$_3$O$_4$ material [18,27]). As a result, the modeled defectuous LBCO film presents two different types of CoO planes: one is Co^{+2}O^{-2}, which is neutral, and the other one is Co^{+3}O$_2^{-2}$, which is charged -1. The electric dipoles centered in the LaO planes being in-between Co^{+2}O^{-2} and Co^{+3}O$_2^{-2}$ planes therefore experience an internal electric field being down (i.e., oriented towards the Co^{+3}O$_2^{-2}$ planes), while the electric dipoles centered in the BaO planes being in-between Co^{+2}O^{-2} and Co^{+3}O$_2^{-2}$ planes feel an internal electric field being up (i.e., oriented towards the Co^{+3}O$_2^{-2}$ planes). As evidenced by our DFT calculations reported in Table III, LaO-centered (respectively, BaO-centered) dipoles are therefore created antiparallel (respectively, parallel) to the growth direction because of these internal fields. Similarly, since BaO planes are neutral while LaO planes are charged $+1$, Co(T)O-centered [respectively, Co(O)O$_2$-centered] dipoles are aligned along (respectively, opposite to) the growth direction because of internal fields. This electrostatically-driven formation of the out-of-plane polarization also provides an explanation for another of our predictions that has not been discussed yet, namely why we did not find any stable state for which this out-of-plane component is reverted, that is, it points up rather than down.

We also numerically found that the ground state of the defectuous LBCO compound is doubly degenerate, with the resulting two states having the same out-of-plane polarization while having *opposite* in-plane polarizations. To understand its occurrence, Fig. 4 shows a top view of the atomic structure of the two degenerate ground states. Let us first indicate again that the defectuous LaBaCo$_2$O$_5$ system possesses two different types of Co ions: Co ions that are denoted as Co(O) and experience an octahedral environment due to their six neighboring oxygen atoms, leading to in-plane and out-of-plane Co-O bonds being 1.98 and 2.38 Å, respectively; Co ions

TABLE III. Born effective charges (Z_o), cation-oxygen rumpling (δ_o) and corresponding contribution of the out-of-plane component of the polarization (P_o) for the different (001) layers in the L2 structure of LaBaCo$_2$O$_5$.

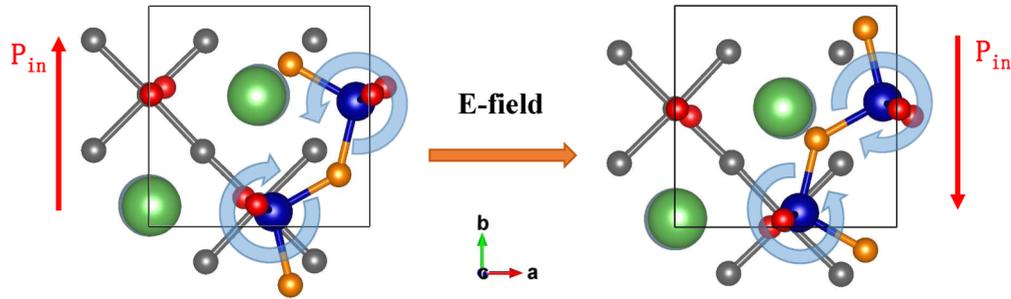| Layer	La-O	Ba-O	Co(T)-O	Co(O)-O$_2$
Z_o (e)	4.26 (La) and –2.92 (O)	3.14 (Ba) and –3.18 (O)	3.75 (Co) and –1.97s8 (O)	1.33 (Co) and (–2.30,–2.09) for O
δ_o (Å)	–0.687	0.512	0.184	–0.165
P_o(μC/cm^2)	–20.9	20.1	9.5	–10.0

FIG. 4. Top view of the atomic structures of the two degenerate ground states of LaBaCo$_2$O$_5$. The left panel and right panel configurations possess in-plane polarization P_{in} along the pseudocubic [110] direction and [$\bar{1}\bar{1}$0] direction, respectively. The oxygen atoms in the Co(O)O$_2$ plane (Co in an octahedral environment) are shown in gray, while those belonging to the Co(T)O plane (Co in a tetrahedral environment) are depicted in orange. The other oxygen atoms are shown in red, while blue spheres correspond to Co ions. The light blue and green spheres represent Ba and La ions, respectively.

that are coined Co(T) and that are tetrahedrally coordinated (they are located at the center of a CoO$_4$ tetrahedron), with resulting Co-O bonds being mainly parallel to the in-plane and out-of-plane directions of 1.92 and 1.80 Å, respectively. In Fig. 4, oxygen atoms belonging to the Co(O)O$_2$ planes are represented in gray while those in the Co(T)O planes are drawn in orange. One can clearly see that, the oxygen ions belonging to the Co(T)O planes (which are also the planes possessing oxygen vacancies) do not have the same in-plane atomic coordinates than the oxygen ions of the Co(O)O$_2$ planes. Such motions can be thought as causing the CoO$_4$ tetrahedra to rotate about the [001] direction in clockwise or anticlockwise fashion, and result in the existence of an in-plane polarization, P$_{in}$. Interestingly, P$_{in}$ is along the pseudocubic [110] direction *versus* the pseudocubic [$\bar{1}\bar{1}$0] direction in the left and right panels of Fig. 4, respectively, because the rotation about the [001] direction of the CoO$_4$ tetrahedra is reversed between these left and right panels. The configurations in these two panels have therefore the same energy and the same space group but opposite in-plane polarizations. Interestingly, the energy barrier between these two states is calculated to be 66 meV per CoO$_4$ tetrahedra, which is similar to the barrier energy of 76 meV per five atoms between the two states of opposite polarization in the ferroelectric prototype PbTiO$_3$ [28]. Therefore applying an electric field to defectuous LBCO should result in the reversal of this in-plane polarization via the switching between these two configurations, which makes such system ferroelectric.

D. Understanding the differences in properties between LaBaCo$_2$O$_6$ and LaBaCo$_2$O$_5$

Let us now try to better understand our predictions about the difference in electronic properties (metal *versus* insulator) and in magnetic orderings (ferromagnetic *versus* G-type antiferromagnetic) between the defect-free LaBaCo$_2$O$_6$ and the defectuous LaBaCo$_2$O$_5$ systems. For that, their computed electronic density of states is shown in Figs. 5(a)–5(d). Note that spin-orbit interactions are not included in these computations. Figure 5(a) clearly demonstrates that the FM defect-free LaBaCo$_2$O$_6$ material is indeed predicted to be metallic since its Fermi energy (chosen as the zero in energy) falls in within bands. Its highest occupied valence states are

made of O $2p$ electrons and Co $3d$ electrons. Figure 5(a) further indicates that the Co $3d$ t_{2g} orbitals heavily contribute (along with a small amount of O $2p$ electrons, not shown here) to the states located between -1 and ~1 eV, including the Fermi level. As a result, the Co $3d$ electrons of LaBaCo$_2$O$_6$ near the Fermi level are rather delocalized in the real space.

Regarding the G-type AFM LaBaCo$_2$O$_5$ system, Co(O) is numerically found to have a magnetic moment of $\sim2.5\,\mu_B$, while Co(T) possesses a magnetic moment of $\sim2.8\,\mu_B$. The G-type AFM LaBaCo$_2$O$_5$ compound is calculated to be an insulator with a small band gap of the order of 0.56 eV, as evidenced in Fig. 5(b). Like in defect-free LaBaCo$_2$O$_6$, (i) the highest occupied states are made of O 2p electrons (not shown here) mixed with Co $3d$ t_{2g} orbitals [see Fig. 5(d)]; (ii) the lowest unoccupied conduction states (in the energy range of ~0.56 to ~3 eV above the Fermi energy) are mostly made of Co $3d$ orbitals being mixed with a few percentage of O $2p$ electrons. Figures 5(c) and 5(d) also reveal that the occupied states being near the valence-band maximum involve the t_{2g} states of the "octahedral" Co(O) ion while the unoccupied states located close to the conduction-band minimum are rather made of the t_2 orbitals of the tetrahedra Co(T) ion, which therefore explains why, unlike the defect-free LaBaCo$_2$O$_6$ compound (that has only one type of Co ion), LaBaCo$_2$O$_5$ is insulator and possesses localized Co $3d$ electrons.

Let us now try to understand the origin for the difference in magnetic ordering between LaBaCo$_2$O$_6$ and LaBaCo$_2$O$_5$, by using a simple model. For that, Figs. 5(e) and 5(f) show the schematic description of the Co $3d$ energy level of these two oxides, respectively. The crystal field (octahedral environment) splits the $3d$ orbitals of the Co ions in LaBaCo$_2$O$_6$ in the manner shown in Fig. 5(e). Here, each Co ion has a nominal ionic charge of $+3.5$ in order to make the whole system neutral. As a result, every Co ion has five $3d$ electrons that can be arranged in the spin configuration shown in Fig. 5(e) *and* there is an additional electron that is shared by two neighboring Co ions in LaBaCo$_2$O$_6$. Such additional electron is the so-called itinerant electron, and can thus transfer back and forth from one Co ion to the other one [as schematized by the green dashed dot curve line of Fig. 5(e)]. In the schematization of Fig. 5(e), LaBaCo$_2$O$_6$ is therefore metallic and ferromagnetic, as computationally found. According to this picture, each Co ion should have an averaged magnetic

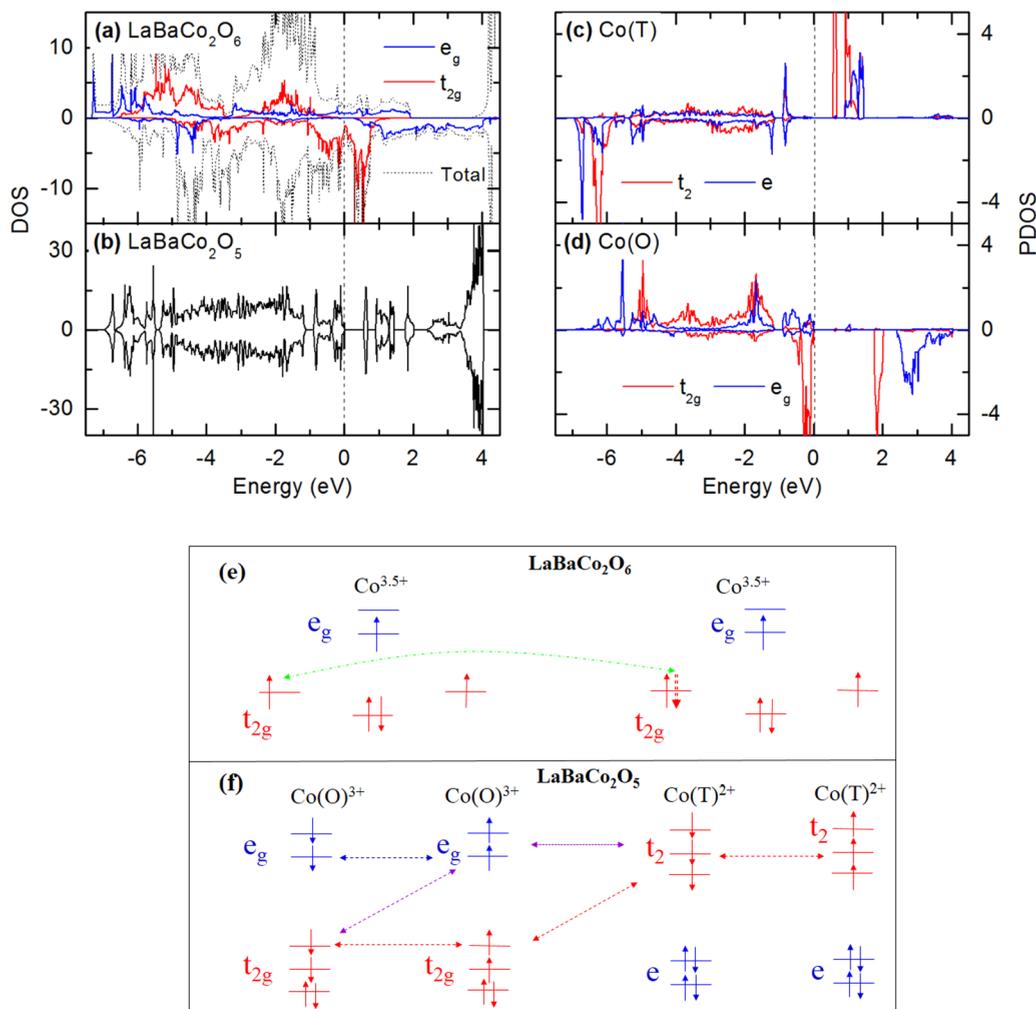FIG. 5. Computed electronic density of states and resulting proposed simple model. (a) shows the total density of states of LaBaCo$_2$O$_6$ as well as e and t_2 states of Co ions in LaBaCo$_2$O$_6$. (b) shows the total density of states of LaBaCo$_2$O$_5$. (c) and (d) report e and t_2 orbitals density of states of the Co(T) and Co(O) in LaBaCo$_2$O$_5$, respectively. In (a)–(d), the zero energy is set at the Fermi level, and positive and negative values of these density of states correspond to spin-up and spin-down channels, respectively. (e) and (f) depict the schematic description for the energy levels of the Co $3d$ orbitals in LaBaCo$_2$O$_6$ and LaBaCo$_2$O$_5$ oxides, respectively. The solid blue and red solid arrows are for the e and t_2 electrons. In (e), the red dashed arrow corresponds to the itinerant electron of LaBaCo$_2$O$_6$, and the green curved line symbolizes the transfer of the itinerant electron. Distorted CoO$_6$ octahedral and CoO$_4$ tetragonal entities both exist in LaBaCo$_2$O$_5$, therefore leading to Co ions having either a $+3$ or a $+2$ nominal charge, as indicated in (f). The different super-exchange interactions are represented by dashed lines in (f).

moment of $5/2 = 2.5\,\mu_{\rm B}$, which is rather consistent with the first-principles value of $2.2\,\mu_{\rm B}$.

On the other hand, the two different types of crystal field existing in LaBaCo$_2$O$_5$ (because of octahedral *versus* tetrahedral environment) split the $3d$ orbitals of Co ions in the manner shown in Fig. 5(f): the t_{2g} orbitals have lower energy than the e_g orbitals in the Co(O) sites, while the reverse situation applies to the Co(T) sites. In addition and as indicated above, the Co(O) and Co(T) ions are expected to have a nominal charge of $+3$ and $+2$, respectively, which leads to each Co(O) ion having six $3d$ electrons, while there are seven $3d$ electrons surrounding each Co(T) ion. Figure 5(f) shows the proposed simple model of the electron configurations for Co(O) and Co(T) and the corresponding exchange interactions. The e_g and t_{2g} orbitals in Co(O) and half-filled t_2 orbitals in Co(T) lead to three kinds of interactions, Co(O)-Co(T), as well as Co(O)-Co(O) and Co(T)-Co(T) interactions. As is

shown in Fig. 5(f), for Co(O)-Co(T), there are super-exchange interactions between Co(O)'s e_g and Co(T)'s t_2, as well as between Co(O)'s t_{2g} and Co(T)'s t_2. For Co(O)-Co(O), there are e_g-e_g, t_{2g}-t_{2g}, and t_{2g}-e_g super-exchange interactions. Finally, for Co(T)-Co(T), there is only the t_2-t_2 super-exchange interaction. As a result and according to the Goodenough-Kanamori rule [29,30], all these super-exchange interactions are antiferromagnetic in nature, and thus leads to an overall G-type AFM ordering. This occupation of orbitals lead to $3\,\mu_{\rm B}$ for Co(T) and $4\,\mu_{\rm B}$ for Co(O). Our DFT calculations does confirm this value close to $3\,\mu_{\rm B}$ for Co(T) (it is $\sim 2.8\,\mu_{\rm B}$), but provides a smaller than expected value for the magnetization of Co(O) (it is numerically found to be $\sim 2.5\,\mu_{\rm B}$ rather than $4\,\mu_{\rm B}$). Such latter discrepancy arises from the fact that the $3d$ orbitals of Co(O) hybridize with the oxygen orbitals and that such hybridization is not included in the model associated with Fig. 5(f). Note that such hybridization also explains why the
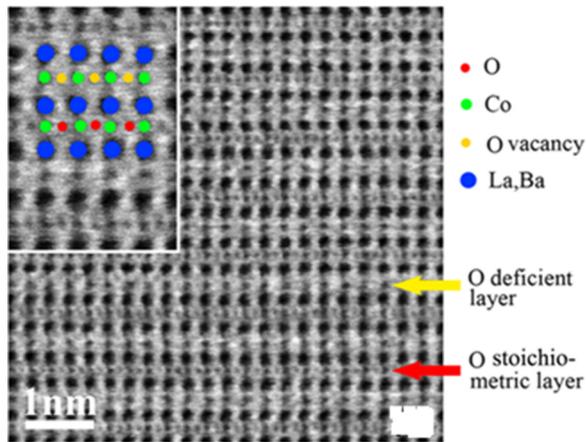
FIG. 6. Annular bright field image of vacuum annealed LBCO thin film.

magnetic moment of Fe ions in $BiFeO_3$ is found to be close to $4\,\mu_B$ by experiments [31] and first-principles calculations [32], while an energetic diagram similar to Figs. 5(e) and 5(f) and only involving $3d$ orbitals, yields a higher value of $5\,\mu_B$.

We also conducted experiments, mostly to demonstrate that defect-engineering can indeed been conceived in LBCO (but also to help us determine which structure to theoretically investigate). We expose as-grown LBCO thin film grown on a Nb-doped $SrTiO_3$ (Nb:STO) substrate under oxygen annealing treatments but also under vacuum post annealing treatments. Annular bright field (ABF) scanning transmission electron microscopy (STEM) imaging techniques were performed in cross-section samples. As shown in Fig. 6 and discussed in Ref. [23], the ABF image is consistent with the existence

of the (novel) defectuous $LaBaCo_2O_5$ structure with ordered oxygen vacancies we computationally investigated. As further indicated in Ref. [23], measurements also confirm our predictions that defectuous $LaBaCo_2O_5$ has a weak magnetization of the order of $0.02-0.04\,\mu_B$ per f.u. and an axial ratio close to 1.02, while defect-free $LaBaCo_2O_6$ is ferromagnetic with an axial ratio smaller than 1.

IV. CONCLUSIONS

First-principles calculations were employed to reveal the possibility of transforming LBCO systems from ferromagnetic and metallic to antiferromagnetic, insulator and ferroelectric, via the creation of ordered oxygen vacancies. Analysis of the results also explains the reasons behind such striking transformations. Finally, growths and measurements were conducted to demonstrate that defect-engineering is practical in these systems and to confirm some of our predictions, which is therefore a promising route to design materials with novel properties and new multiferroics.

[1] X. Xie, Y. Li, Z.-Q. Liu, M. Haruta, and W. Shen, Nature (London) **458**, 746 (2009).

[2] G. Kim, S. Wang, A. J. Jacobson, Z. Yuan, W. Donner, C. L. Chen, L. Reimus, P. Brodersen, and C. A. Mims, Appl. Phys. Lett. **88**, 024103 (2006).

[3] Y.-M. Kim, J. He, M. D. Biegalski, H. Ambaye, V. Lauter, H. M. Christen, S. T. Pantelides, S. J. Pennycook, S. V. Kalinin, and A. Y. Borisevich, Nat. Mater. **11**, 888 (2012).

[4] J. Liu, M. Liu, G. Collins, C. L. Chen, X. N. Jiang, W. Q. Gong, A. J. Jacobson, J. He, J. C. Jiang, and E. I. Meletis, Chem. Mater. **22**, 799 (2010).

[5] V. G. Bhide, D. S. Rajoria, C. N. R. Rao, G. R. Rao, and V. G. Jadhao, Phys. Rev. B **12**, 2832 (1975).

[6] F. Fauth, E. Suard, V. Caignaert, B. Domenges, I. Mirebeau, and L. Keller, Eur. Phys. J B **21**, 163 (2001).

[7] J. B. Goodenough, J. Phys. Chem. Solids **6**, 287 (1958).

[8] A. Maignan, C. Martin, D. Pelloquin, N. Nguyen, and B. Raveau, J. Solid State Chem. **142**, 247 (1999).

[9] B. Raveau, Phil. Trans. R. Soc. A **366**, 83 (2008).

[10] M. M. Seikh, C. Simon, V. Caignaert, V. Pralong, M. B. Lepetit, S. Boudin, and B. Raveau, Chem. Mater. **20**, 231 (2008).

[11] M. Liu, J. Liu, G. Collins, C. R. Ma, C. L. Chen, J. He, J. C. Jiang, E. I. Meletis, A. J. Jacobson, and Q. Y. Zhang, Appl. Phys. Lett. **96**, 132106 (2010).

[12] M. Liu, C. R. Ma, J. Liu, G. Collins, C. L. Chen, J. He, J. C. Jiang, E. I. Meletis, L. Sun, A. J. Jacobson *et al.*, ACS Appl. Mater. Interfaces **4**, 5524 (2012).

[13] C. R. Ma, M. Liu, G. Collins, J. Liu, Y. M. Zhang, C. L. Chen, J. He, J. C. Jiang, and E. I. Meletis, Appl. Phys. Lett. **101**, 021602 (2012).

[14] C. R. Ma, M. Liu, G. Collins, H. B. Wang, S. Y. Bao, X. Xu, E. Enriquez, C. L. Chen, Y. Lin, and M. H. Whangbo, ACS Appl. Mater. Interfaces **5**, 451 (2013).

[15] W. Donner, C. L. Chen, M. Liu, A. J. Jacobson, Y. L. Lee, M. Gadre, and D. Morgan, Chem. Mater. **23**, 984 (2011).

[16] E.-L. Rautama, P. Boullay, A. K. Kundu, V. Caignaert, V. Pralong, M. Karppinen, and B. Raveau, Chem. Mater. **20**, 2742 (2008).

[17] T. Nakajima, M. Ichihara, and Y. Ueda, J. Phys. Soc. Jpn. **74**, 1572 (2005).

[18] L. Chen, Y. R. Yang, and X. K. Meng, Appl. Phys. Lett. **102**, 203102 (2013).

[19] J. P. Perdew, A. Ruzsinszky, G. I. Csonka, O. A. Vydrov, G. E. Scuseria, L. A. Constantin, X. L. Zhou, and K. Burke, Phys. Rev. Lett. **100**, 136406 (2008).

[20] G. Kresse and D. Joubert, Phys. Rev. B **59**, 1758 (1999).

[21] J. Heyd, G. E. Scuseria, and M. Ernzerhof, J. Chem. Phys. **124**, 219906 (2006).

[22] R. D. King-Smith and D. Vanderbilt, Phys. Rev. B **47**, 1651 (1993).

[23] See Supplemental Material at http://link.aps.org/supplemental/10.1103/PhysRevB.95.165132 for growth and characterization of epitaxial LBCO films.

[24] S. Sengodan, S. Choi, A. Jun, T. H. Shin, Y.-W. Ju, H. Y. Jeong, J. Shin, J. T. S. Irvine, and G. Kim, Nat. Mater. **14**, 205 (2015).

[25] Y. Ito, R. F. Klie, N. D. Browning, and T. J. Mazanec, J. Am. Ceram. Soc. **85**, 969 (2002).

[26] H. Sakai, J. Fujioka, T. Fukuda, D. Okuyama, D. Hashizume, F. Kagawa, H. Nakao, Y. Murakami, T. Arima, A. Q. R. Baron *et al.*, Phys. Rev. Lett. **107**, 137601 (2011).

[27] J. Chen, X. Wu, and A. Selloni, Phys. Rev. B **83**, 245204 (2011).

[28] S. P. Beckman, X. Wang, K. M. Rabe, and D. Vanderbilt, Phys. Rev. B **79**, 144124 (2009).

[29] J. B. Goodenough, Phys. Rev. **100**, 564 (1955).

[30] J. Kanamori, J. Phys. Chem. Solids **10**, 87 (1959).

[31] P. Fischer, M. Polomska, I. Sosnowska, and M. Szymanski, J. Phys. C **13**, 1931 (1980).

[32] J. B. Neaton, C. Ederer, U. V. Waghmare, N. A. Spaldin, and K. M. Rabe, Phys. Rev. B **71**, 014113 (2005).